

See discussions, stats, and author profiles for this publication at: <https://www.researchgate.net/publication/23152876>

# Quantum Mechanical Calculation of Energy Dependence of OCl/OH Product Branching Ratio and Product Quantum State Distributions for the O( 1 D ) + HCl Reaction on All Three Contribut...

ARTICLE *in* THE JOURNAL OF PHYSICAL CHEMISTRY A · SEPTEMBER 2008

Impact Factor: 2.69 · DOI: 10.1021/jp803673y · Source: PubMed

---

CITATIONS

14

READS

176

## 8 AUTHORS, INCLUDING:



Huan Yang

Shandong University

17 PUBLICATIONS 140 CITATIONS

[SEE PROFILE](#)



Shinkoh Nanbu

Sophia University

107 PUBLICATIONS 897 CITATIONS

[SEE PROFILE](#)



Hiroki Nakamura

National Chiao Tung University

238 PUBLICATIONS 4,089 CITATIONS

[SEE PROFILE](#)



Gabriel Balint-Kurti

University of Bristol

186 PUBLICATIONS 4,675 CITATIONS

[SEE PROFILE](#)

# Quantum Mechanical Calculation of Energy Dependence of OCl/OH Product Branching Ratio and Product Quantum State Distributions for the O(<sup>1</sup>D) + HCl Reaction on All Three Contributing Electronic State Potential Energy Surfaces

Huan Yang,<sup>†</sup> Ke-Li Han,<sup>†</sup> Shinkoh Nanbu,<sup>‡</sup> Hiroki Nakamura,<sup>§</sup> Gabriel G. Balint-Kurti,<sup>||</sup> Hong Zhang,<sup>†</sup> Sean C. Smith,<sup>†</sup> and Marlies Hankel<sup>\*,†</sup>

State Key Laboratory of Molecular Reaction Dynamics, Dalian Institute of Chemical Physics, Chinese Academy of Sciences, Dalian 116023, China, Research Institute for Information Technology, Kyushu University, 6-10-1 Hakozaki, Higashi-ku Fukuoka 812-8581, Japan, Institute for Molecular Science, Myodaiji, Okazaki 444-8585, Japan, School of Chemistry, University of Bristol, Bristol BS8 1TS, United Kingdom, and Centre for Computational Molecular Science, Australian Institute for Bioengineering and Nanotechnology, The University of Queensland, QLD 4072, Australia

Received: April 27, 2008; Revised Manuscript Received: June 9, 2008

OCl/OH product branching ratios are calculated as a function of total energy for the O(<sup>1</sup>D) + HCl reaction using quantum wavepacket methods. The calculations take account of reaction on all the three electronic state potential energy surfaces which correlate with both reactants and products. Our results show that reaction on the excited electronic state surfaces has a large effect on the branching ratio at higher energies and that these surfaces must therefore be fully taken into account. The calculations use the potential energy surfaces of Nanbu and co-workers. Product vibrational and rotational quantum state distributions are also calculated as a function of energy for both product channels. Inclusion of the excited electronic state potential energy surfaces improves the agreement of the predicted product vibrational quantum state distributions with experiment for the OH product channel. For OCl agreement between theory and experiment is retained for the vibrational quantum state distributions when the excited electronic state potential energy surfaces are included in the analysis. For the rotational state distributions good agreement between theory and experiment is maintained for energies at which experimental results are available. At higher energies, above 0.7 eV of total energy, the OCl rotational state distributions predicted using all three electronic state potential energy surfaces shift to markedly smaller rotational quantum numbers.

## I. Introduction

The reaction of electronically excited oxygen with hydrogen chloride has been the focus of several experimental<sup>1–12</sup> and theoretical studies.<sup>13–36</sup> The reaction plays an important role in the modeling of atmospheric chemistry and presents an interesting system for the study of fundamental reaction dynamics. The chemical and photochemical stability of HCl make it an ideal sink for chlorine in most parts of the atmosphere. This acts to offset the potentially damaging effect of chlorine-releasing chemicals, such as the chlorofluorocarbons particularly in that part of the ozone layer below about 30–35 km. Above this altitude, however, O(<sup>1</sup>D) is generated, for example, by solar photolysis of ozone or water. O(<sup>1</sup>D) reacts with HCl, releasing OH radicals and Cl atoms, regenerating reactive Cl from the HCl stratospheric sink. Because both OH and Cl are involved in separate reactions which consume ozone, the O(<sup>1</sup>D) + HCl reaction has been implicated in the complex chemistry governing the destruction of the earth's ozone layer.<sup>4,5</sup>

\* To whom correspondence should be addressed. E-mail: m.hankel@uq.edu.au.

<sup>†</sup> State Key Laboratory of Molecular Reaction Dynamics, Dalian Institute of Chemical Physics, Chinese Academy of Sciences.

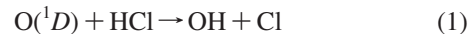
<sup>‡</sup> Research Institute for Information Technology, Kyushu University.

<sup>§</sup> Institute for Molecular Science.

<sup>||</sup> School of Chemistry, University of Bristol.

<sup>†</sup> Centre for Computational Molecular Science, Australian Institute for Bioengineering and Nanotechnology, The University of Queensland.

For the O(<sup>1</sup>D) + HCl reaction there are two competing product channels:



where (1) is the dominant channel with the reactivity of (2) being about 30% compared to (1). It is accepted that reaction (1) produces vibrationally excited OH. This was first observed in 1961 by Basco and Norrish<sup>1</sup> in flash photolysis experiments of ozone and was confirmed nearly 20 years later by Luntz<sup>2</sup> using laser-induced fluorescence. Kruus et al.<sup>4</sup> and Park et al.<sup>5</sup> reported vibrational state distributions for the OH product measured by infrared chemiluminescence and laser-induced fluorescence, respectively. Kruus et al.<sup>4</sup> reported an inverted vibrational state distribution which peaks at  $v' = 3$  with nearly equal population for  $v' = 4$ . The peak is very pronounced with the populations for the other states,  $v' = 1$  and  $v' = 2$ , being much smaller. A similar distribution at an average total energy<sup>37</sup> of 0.5 eV has been reported by Park et al.<sup>5</sup> showing a very pronounced peak at  $v' = 4$ . In a recent crossed molecular beam imaging study, Kohguchi and Suzuki<sup>11</sup> also reported an OH vibrational distribution peaking at  $v' = 3, 4$  at a total energy of 0.45 eV. The population of  $v' = 0$  and  $v' = 5$  was reported to be negligible.

Wine et al.<sup>3</sup> measured the absolute rate constants at 297 K, and the authors estimated the branching ratio of the two reaction product arrangement channels, OCl + H and OH + Cl, as 0.36

$\pm 0.10$ . Balucani et al.<sup>6</sup> studied the  $O(^1D) + HCl \rightarrow OCl + H$  reaction in a crossed-beam experiment. They estimated a lower limit for the branching ratio of  $\sigma_{OCl}/\sigma_{OH} \geq 0.34 \pm 0.1$  at a total energy of 0.72 eV. The authors also predict that, in contrast to the OH product vibrational state distribution, the OCl vibrational state distribution is not inverted. Matsumi et al.<sup>7</sup> studied both reactions and used the resonance-enhanced multiphoton ionization technique to detect the atomic products. They report a branching ratio of  $0.24 \pm 0.06$  at a total energy of 0.52 eV. In two more studies Matsumi et al.<sup>8,9</sup> measured the vibrational and rotational state distributions of the OCl molecule employing vacuum ultraviolet laser-induced fluorescence. The authors report that the vibrational distribution at a total energy of 0.554 eV for  $OCl(v' = 0-3)$  is not inverted, with  $v' = 0$  being the most populated state and the population for  $v' = 3$  being zero.

Five electronic states correlate adiabatically with the reactants of which three,  $1^1A'$ ,  $1^1A''$ , and  $2^1A'$  (for simplicity, we will omit the singlet superscript), also correlate with at least one of the two possible products. Several potential energy surfaces (PES) are available for the ground electronic state.<sup>13,14,22,26,30</sup> In 1984, Schinke<sup>13</sup> produced an analytical fit to ab initio data calculated by Liu.<sup>38</sup> This is called the BLRS PES. Ten years later, Laganá et al.<sup>14</sup> reported a new ground electronic state PES that had been fitted, using the LAGROBO model, to limited ab initio and spectroscopic information available in the literature. To improve the agreement with the available experimental data, the authors performed ab initio calculations and produced a new fitted surface, the BO or H1 PES.<sup>15</sup> In 2000, Laganá et al.<sup>22</sup> performed additional calculations to supplement the ab initio points and produced an improved version of the BO (H1) PES, hereafter called H2 PES.<sup>22</sup> In 1998, Skokov et al.<sup>16</sup> constructed a semi global ab initio surface of near spectroscopic accuracy for HOCl.<sup>18</sup> In 1999, the same authors extended the ab initio calculations to include the HClO isomer and the OCl + H dissociation channel and produced a global surface, PSB1.<sup>20</sup> A new fit to the PSB1 data produced a new improved analytical ground electronic state surface, called PSB2.<sup>25,26</sup> The most recently available surfaces are those of Nanbu et al.<sup>30</sup> who reported ab initio results for all three surfaces. These surfaces are denoted as the N1 potential energy surfaces. To improve the accuracy of the N1 PESs for the calculations of the HOCl spectrum<sup>39,40</sup> additional ab initio points for each electronic state have been added mainly in the vicinity of the HOCl equilibrium to refine the N1 PESs. The new refined PESs are denoted N2. Figure 1 shows a schematic representation of the energetics of the three electronic states of the N2 PESs.

Most theoretical investigations of the  $O(^1D) + HCl$  reaction dynamics have been carried out using only the ground electronic state PES. The product OH vibrational quantum state distributions obtained by Schinke<sup>13</sup> on the BLRS PES at 0.3 eV peak at  $v' = 2, 3$ . Also, the OH rotational state distributions for the first six vibrational states peaked at high rotational states. The range of product states populated shifts to lower rotational quantum numbers for higher product vibrational states. Lin et al.<sup>23,24,33</sup> investigated the reaction using the Reactive Infinite Order Sudden Approximation (RIOSA). The OH vibrational quantum state distributions obtained show a pronounced peak at  $v' = 4$  and do not change significantly with energy.

Laganá et al.<sup>14</sup> performed quasi classical trajectory (QCT) calculations on the LAGROBO PES. The resulting OH product vibrational quantum state distributions are inverted and peak at  $v' = 1$  with the population for  $v' = 3$  and 4, which are the most populated states in the experimental measurements, being small. QCT calculations employing the H1 PES<sup>15</sup> produced OH

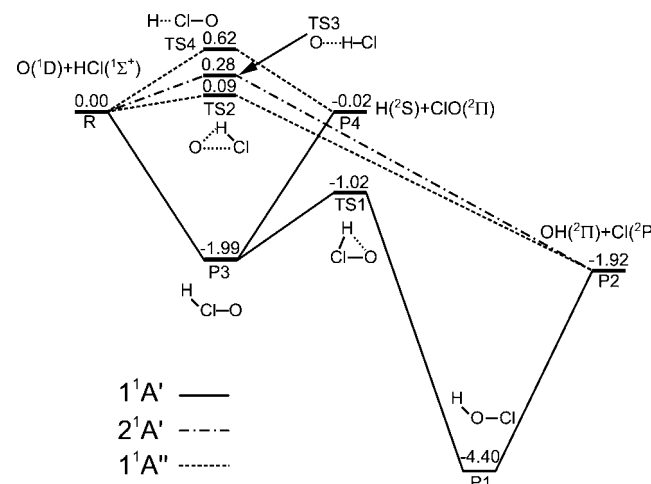


**Figure 1.** Schematic diagram of the wells and transition states for all three electronic states,  $1^1A'$ ,  $1^1A''$ , and  $2^1A'$ , involved in the  $O(^1D) + HCl$  reaction.

product vibrational quantum state distributions that peak at  $v' = 0$  with the populations of the higher states decreasing steadily. Finally, employing the H2 PES, the OH product vibrational state distributions are found to be inverted peaking at  $v' = 2$ .<sup>22</sup> Piermarini et al. carried out calculations for the H2 PES employing the real wavepacket approach,<sup>27,28</sup> and found that the OH product vibrational state distributions obtained from the quantum calculations differed from those obtained from the QCT calculations. The distributions from the quantum calculations peaked at higher vibrational states,  $v' = 4$ , achieving better agreement with experiment. Product rotational state distributions for the first six vibrational states of OH are inverted peaking at high rotational states. The range of populated rotational states shifts to lower  $j'$  quantum numbers with increasing  $v'$ . The OCl rotational state distributions extend to even higher rotational states but with relatively equal population of all of the rotational states.<sup>28</sup>

Christoffel et al.<sup>21</sup> performed quantum ( $J = 0$ ) and QCT calculations employing the PSB1 PES. The OH product vibrational state distribution obtained from the QCT calculations is in reasonable agreement with experiment, peaking at  $v' = 2$  with  $v' = 3$  having a similar population. Calculations on the PSB2 PES<sup>29</sup> show good agreement for the vibrational state distributions with the one for OH peaking at  $v' = 3$  compared to  $v' = 2$  on the PSB1 PES.

Kamisaka et al. performed time-independent quantum dynamical calculations for all three electronic states of the N1 PES.<sup>31,32</sup> The vibrational state distributions for OH are inverted peaking at  $v' = 4$ . In a recent quantum dynamical study, the present authors employed the N2 PES<sup>41</sup> to study the reaction probability and also the product quantum state distributions at the two fixed energies.<sup>6,7</sup>

Laganá et al.<sup>14</sup> performed QCT calculations on the LAGROBO PES. The calculated branching ratios at 0.72 and 0.52 eV total energy are 0.59 and 0.47 respectively. The first value agrees well with the experimentally observed<sup>6</sup> lower limit of  $0.34 \pm 0.1$  but the second value is much larger than the experimental value<sup>7</sup> of  $0.24 \pm 0.06$  at that energy. The branching ratios calculated on the H1 PES<sup>15</sup> of  $0.24 \pm 0.09$  at 0.52 eV and  $0.36 \pm 0.08$  at 0.72 eV total energy agree well with the experimental measurements. The branching ratios obtained using QCT calculations on the H2 PES<sup>22</sup> also agree well with experiment. Piermarini et al. carried out quantum mechanical calculations employing the real wavepacket approach<sup>27,28</sup> and

obtained good agreement with the experimental branching ratio at 0.72 eV. Christoffel et al.<sup>21</sup> performed quantum ( $J = 0$ ) and QCT calculations on the PSB1 PES. The calculated branching ratios obtained from both methods agreed well with the experimental values. Christoffel et al.<sup>29</sup> then carried out QCT calculations on the PSB2 PES. They found that the quantum and QCT branching ratios for the PSB2 PES were much smaller than the experimental values. Initial rotational excitation was found to increase the OCl cross section but to decrease the OH cross section therefore leading to an increase of the branching ratio. A similar effect was found when going from  $v = 0$  to  $v = 1$ . Kamisaka et al. performed time-independent quantum dynamics calculations for all three electronic states of the N1 PES.<sup>31,32</sup> The branching ratio obtained (including the contributions from all three electronic states) ranged from 0.23 to 0.32 in the energy range considered, which compares well with the experimental results. They also found that initial state excitation decreases the reactivity to form OH and increases it for OCl on the ground electronic state. For the two excited electronic states, the probability of producing OH products is increased while that for OCl is decreased.

All theoretical studies to date show agreement with experiment on the OCl product vibrational state distributions, peaking at  $v' = 0$  with the populations decreasing with increasing  $v'$ . Also, there is general agreement that the OH rotational state distributions are inverted, populating mostly high rotational states, while the distributions for OCl are broader, though they are also found to peak at high  $j'$  quantum numbers. However, the OH vibrational state distributions arising from most available PESs are not hot enough, peaking at  $v' = 2, 3$ . Only quantum calculations employing the H2, N1, and N2 PESs have achieved agreement with experiment reporting distributions peaking at  $v' = 3, 4$ . In general, good agreement of theoretical branching ratios with experiment was obtained for all available PES. However, the branching ratio obtained for the PSB2 PES<sup>29</sup> at 0.72 eV is too small and the quantum mechanically calculated branching ratio obtained for the H2 PES<sup>27,28</sup> is larger (close to 1) than the corresponding experimental value at 0.52 eV. It should be noted that also the branching ratio at 0.72 eV is close to 1 for the H2 surface.

The reaction probabilities for  $J = 0$ , especially for the ground electronic state, are highly structured, therefore the branching ratio and the vibrational state distributions for both products arrangement channels will be strongly energy dependent. In the current paper, we will therefore present branching ratios and vibrational and rotational quantum state distributions as a function of total energy to investigate the energy dependence of these quantities. We will also present results that have been averaged over the three contributing electronic states to investigate their effect on the dynamics. We will discuss the importance of the excited states in the comparison of our theoretical predictions with the experimental data.

Section II briefly gives some of the details of the calculations while section III presents and discusses the resulting branching ratios and product vibrational and rotational quantum state distributions as a function of energy. Section IV summarizes the results and presents the conclusions of the article.

## II. Calculation Details

We have performed quantum state-to-state calculations of reaction probabilities for total angular momentum  $J = 0$  for both product arrangement channels and for all three electronic states employing the N2 PESs as in our previous study.<sup>41</sup> Separate adiabatic calculations were carried out for each

electronic state. The time-dependent real wavepacket method<sup>42–44</sup> was used in the calculations and all parameters were the same as those used in ref 41.

Vibrational state resolved reaction probabilities have been calculated for the lowest ten product vibrational levels of each electronic state and for both product arrangement channels. The probabilities for the lowest seven of these are reported as a function of energy in the next section. Contour maps showing the product rotational quantum state distributions as a function of energy for each of these vibrational states are also presented. Reaction probabilities were evaluated between total energies of 0.1 and 1.1 eV in steps of 0.002 eV. Also presented in the next section are various reaction probabilities averaged over all three electronic states. In this case, results were evaluated over the same energy range but at intervals of 0.1 eV.

Branching ratios are also calculated as a function of total energy, for both the lowest  $1^1A'$  electronic state on its own and also averaged over all three electronic states. The ground electronic state only branching ratio is calculated as  $\rho^{1A'}(E) = \sigma_{OCl}^{1A'}(E)/\sigma_{OH}^{1A'}(E)$ , where  $\sigma_{OCl}^{1A'}(E)$  and  $\sigma_{OH}^{1A'}(E)$  represent the total reaction probability for the OCl and OH product arrangement channel. To calculate the branching ratio averaged over all three contributing electronic states we treat them as being degenerate, giving each of them an equal weight. The averaged branching ratio is then obtained as

$$\rho^{\text{all}}(E) = \frac{\sigma_{OCl}^{1A'}(E) + \sigma_{OCl}^{1A''}(E) + \sigma_{OCl}^{2A'}(E)}{\sigma_{OH}^{1A'}(E) + \sigma_{OH}^{1A''}(E) + \sigma_{OH}^{2A'}(E)} \quad (3)$$

It should be noted here that the contribution  $\sigma_{OCl}^{2A'}(E) = 0$  as the  $2A'$  PES does not correlate with the OCl products. The average vibrational and rotational product state distributions have been obtained as follows:

$$\sigma_{v'}^{\text{all}}(E) = (\sigma_{v'}^{1A'}(E) + \sigma_{v'}^{1A''}(E) + \sigma_{v'}^{2A'}(E))/3 \quad (4)$$

and

$$\sigma_{v'j'}^{\text{all}}(E) = (\sigma_{v'j'}^{1A'}(E) + \sigma_{v'j'}^{1A''}(E) + \sigma_{v'j'}^{2A'}(E))/3 \quad (5)$$

for each product arrangement channel, OH + Cl and OCl + H, separately. Again, the contribution  $\sigma_{v'j'}^{2A'}(E)$  ( $\sigma_{v'j'}^{2A'}(E)$ ) is zero for the OCl + H product arrangement channel.

## III. Results and Discussion

**A. Branching Ratio.** In this section, we will present the branching ratio obtained for the N2 surfaces. Considering first only the ground electronic state surface, the branching ratio at 0.52 eV total energy for the N2 surface is calculated to be  $\rho^{1A'} = 0.307$ , which is just above the experimental<sup>7</sup> value of  $0.24 \pm 0.06$ . The experimental<sup>16</sup> ratio at 0.72 eV represents a lower limit,  $\rho \geq 0.34 \pm 0.1$ . The ratio obtained for the N2 surface at this energy is, 0.354, in very good agreement with the experimental value.

Now, taking the excited electronic states into account the average branching ratio  $\rho^{\text{all}}$  at 0.52 eV is 0.203 and at 0.72 eV we now have 0.231. The ratio,  $\rho^{\text{all}}$ , at 0.52 eV is in excellent agreement with the experimental value, while the one at 0.72 eV is now smaller than the lower limit obtained by experiment.

As the reaction probabilities vary rapidly with energy, investigating the branching ratio at just two fixed energies cannot provide a definitive answer as to whether inclusion of the excited electronic states improve the agreement between experiment and our theoretical predictions. If we look at the branching ratio at two close lying energies, 0.518 and 0.522 eV for example, then

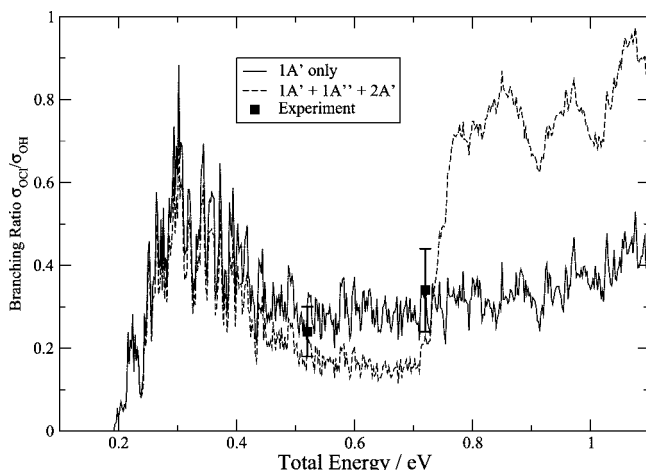


**Figure 2.** Branching ratio,  $\sigma_{\text{OCl}}/\sigma_{\text{OH}}$ , calculated employing the ground electronic state,  $1\text{A}'$  only, and also including the contributions from the excited states,  $1\text{A}''$  and  $2\text{A}'$ . Equal weights for each electronic state have been used. Also included in the figure is the experimental data of  $0.24 \pm 0.06$  at  $0.52$  eV (ref 6) and  $0.34 \pm 0.1$  at  $0.72$  eV (ref 7).

we obtain  $\rho^{1\text{A}'}$  values of  $0.227$  and  $0.332$ , respectively. The first is in very good agreement with experiment while the second one is clearly too large. These variations in the ratio within a narrow energy range are due to the highly structured total reaction probabilities for the ground electronic state as seen in Figure 1 of ref 41.

In this context, one should also consider the relative collision energy spread present in experiment. The difference between the two energies quoted above is only  $0.092$  kcal/mol, which may be less than the uncertainty in the experimental collision energy. It would be desirable to average our predicted branching ratios over the spread of collision energies present in the experiment before making comparisons. To do this, we would need more information on the relative collisional energy spread present in the experiments than we currently possess.

Figure 2 shows the branching ratio calculated using only the  $1\text{A}'$  electronic state PES as a function of energy and also that obtained by averaging over all three electronic state surfaces. The branching ratios show the same sharp structures as the reaction probabilities. If only the ground electronic state is taken into account, then the branching ratio,  $\rho^{1\text{A}'}$ , rises rapidly to an average value of around  $0.6$  and then starts to decrease again. It then levels off between  $0.4$  and  $0.7$  eV at a value of around  $0.3$ . This is due to the flattening out of both product arrangement channel reaction probabilities in this energy range as seen in ref 41. Above  $0.7$  eV,  $\rho^{1\text{A}'}$  rises again due to the increase in the  $\text{OCl} + \text{H}$  reaction probability.  $\rho^{1\text{A}'}$  is in very good agreement with the two experimental<sup>6,7</sup> ratios available, also shown in Figure 2. If we now take the contributions of the excited electronic states into account, then the picture significantly changes. For energies below  $0.4$  eV  $\rho^{\text{all}}$  is very similar to  $\rho^{1\text{A}'}$ . Above  $0.4$  eV  $\rho^{\text{all}}$  continues to decrease and does not level off as does  $\rho^{1\text{A}'}$ . Above  $0.7$  eV, the contribution of the  $1\text{A}''$  state to the  $\text{OCl} + \text{H}$  reaction causes  $\rho^{\text{all}}$  to jump to an average value of nearly  $0.8$  steadily increasing with energy.  $\rho^{\text{all}}$  also agrees well with the two experimental results available.

Comparing  $\rho^{1\text{A}'}$  with  $\rho^{\text{all}}$  in Figure 2 it seems that a better agreement with experiment is achieved for  $\rho^{1\text{A}'}$ . While the experimental value at  $0.72$  eV, being a lower limit, would support a rise in magnitude around this energy, there is as yet no clear experimental evidence for a rapid increase of the

branching ratio as predicted by our calculations using the N2 surfaces when we include the excited states.

Kohguchi et al.<sup>12</sup> recently investigated the energy dependence of reaction (1) by means of crossed molecular beam ion-imaging experiments and QCT calculations employing the N1 surfaces. They measured differential cross sections at  $0.37$ ,  $0.38$ , and  $0.47$  eV total energy. They also calculated differential and total cross sections for  $0.32$ ,  $0.36$ ,  $0.45$ ,  $0.72$ , and  $0.84$  eV total energy to investigate the energy dependence and the influence of the excited states. Good agreement between theory and experiment was achieved using only the ground electronic state. The authors concluded that the effect of the excited electronic states is negligibly below  $0.71$  eV. Our findings show that the  $1\text{A}''$  excited states affects the dynamics leading to the production of OH above around  $0.4$  eV (also see discussion of the OH product vibrational distributions in the next section). This difference might be due to the different versions of the PES employed. However, as reported in our first paper,<sup>41</sup> the thresholds for the production of OH on the  $1\text{A}''$  surface are similar for the N1 and N2 surface. Also, the results obtained on the N1 surfaces, by Kamisaka et al.,<sup>31,32</sup> are larger in magnitude than those reported by us for the N2 surfaces. The differences might be due to the different theoretical methods employed. Also, the present calculations consider  $J = 0$  only. Calculations for  $J > 0$  employing the H2<sup>27</sup> and PSB2<sup>26</sup> surfaces showed that the reaction probability for  $J < 50$  does not change with  $J$  when only the ground electronic state is considered. However, this may no longer be the case if reaction on the excited electronic state PESs is also included in the calculation.

**B. Product Vibrational Quantum State Distributions.** In this section, we report the calculated vibrational state distributions for the OH and OCl products for all three electronic states. The results are presented as product vibrational state resolved reaction probabilities versus total energy, so as to determine the energy dependence of the vibrational state distributions. Figure 3 shows the product vibrational state resolved reaction probabilities for the formation of  $\text{OH} + \text{Cl}$  and  $\text{OCl} + \text{H}$  on all three electronic state PESs. Reaction probabilities for the first seven product vibrational states have been considered for this figure. Results for  $v' = 0-6$  are shown for both product arrangement channels for the ground electronic state. For the production of  $\text{OCl} + \text{H}$  on the  $1\text{A}''$  electronic state  $v' = 6$  has been omitted in panel (d), and  $v' = 0$  and  $v' = 6$  for the production of  $\text{OH} + \text{Cl}$  on the  $1\text{A}''$  and  $2\text{A}'$  electronic states have been omitted in panels (c) and (e) due to their small magnitude and to improve the readability of the figure.

The formation of  $\text{OH} + \text{Cl}$  on the  $1\text{A}'$  state, panel (a), for total energies below  $0.35$  eV vibrational states  $v' = 0-4$  are populated with equal probability. This is interesting as it is commonly accepted that the OH product is predominately produced vibrationally excited in  $v' = 3, 4$  with the population of the other states being much smaller if not negligible. This is only the case for total energies above  $0.4$  eV, where the magnitude of the  $v' = 4$  reaction probability jumps in magnitude by nearly a factor of 2, and then slowly decreases again for energies above  $0.5$  eV. The probabilities for  $v' = 0-3$  decrease with increasing energy above  $0.4$  eV with the one for  $v' = 0$  being the smallest and the one for  $v' = 3$  the largest and the ones for  $v' = 1, 2$  being very similar in magnitude.  $v' = 5$  is populated above  $0.35$  eV and  $v' = 6$  for energies above  $0.69$  eV. The probabilities for most vibrational states shown,  $v' = 0-5$ , become independent of energy above  $0.8$  eV, whereas that for  $v' = 6$  is still increasing but shows a tendency to become

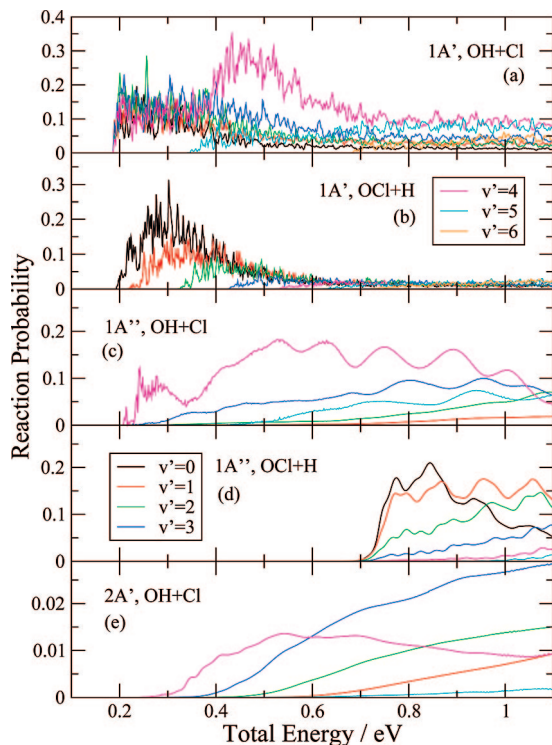


**Figure 3.** Vibrational product state resolved reaction probabilities versus total energy in eV for both product arrangement channels on the  $1\text{ }A'$ , the  $1\text{ }A''$ , and the  $2\text{ }A'$  electronic states.

independent of energy above 1.0 eV. The results show that there seems to be a change in dynamics for energies above 0.4 eV.

Figure 3b shows the reaction probabilities for the  $\text{OCl} + \text{H}$  channel obtained on the  $1\text{ }A'$  state PES. The picture for this product arrangement channel is very different to the one for the  $\text{OH} + \text{Cl}$  channel. All of the product vibrational states, apart from  $v' = 0$  which is nonzero above the initial state energy threshold, display separate thresholds. This is due to the fact that for the N<sub>2</sub> surfaces, the production of  $\text{OCl} + \text{H}$  is nearly thermo neutral. For the  $v' = 0, 1, 2$  states, the reaction probability rises steadily for the first 0.1 eV above threshold and then starts to decrease slowly. For  $v' = 3, 4, 5, 6$ , the rise is more gradual. At an energy of about 0.2 eV above their respective thresholds, the populations of the lower and higher product vibrational states becomes approximately equal. Above 0.8 eV, all six vibrational states examined have roughly equal reaction probabilities.

In Figure 3c, showing the results for the production of  $\text{OH} + \text{Cl}$  on the  $1\text{ }A''$  electronic state, the probability for  $v' = 4$  is the largest for nearly the whole energy range considered here. Only for energies above 1.05 eV is the  $v' = 4$  probability smaller than those for  $v' = 5, 3, 2$ . The second largest probability is that for  $v' = 3$  followed by  $v' = 5, v' = 2$ , and then  $v' = 1$ . The relative ordering of the magnitudes of the reaction probabilities for the different product vibrational states only changes for energies above 1.0 eV. The probability for  $v' = 5$  is nonzero above 0.34 eV. The probabilities for  $v' = 5, 4, 3$  show the same broad structures as the total reaction probabilities, especially for higher energies. The probabilities for  $v' = 2, 1$  are smooth increasing linearly with energy. The probabilities for  $v' = 4, 3$  drop off sharply for energies above 1.0 eV. From panel (c) it seems that several of the vibrational state probabilities show a threshold to reaction but it should be noted here that the probabilities for  $v' = 0-4$  are nonzero above 0.21 eV. The larger magnitude of the probabilities for the higher vibrational states

**TABLE 1: Experimental Product Vibrational Distributions<sup>a</sup>**

	$\text{OH}(v')^b$	$\text{OH}(v')^c$	$\text{OCl}(v')^d$
$v' = 0$		0.0	0.54
$v' = 1$	0.065	0.03	0.31
$v' = 2$	0.135	0.25	0.15
$v' = 3$	0.45	0.3	0.0
$v' = 4$	0.35	0.42	

<sup>a</sup> Numbers for  $\text{OCl}(v')$ , third column, have been taken straight from the text in ref 8. The numbers for  $\text{OH}(v')$  that are presented in the first column have been adapted from Figure 2 of ref 4, using the  $\langle Z_{\text{GK}} \rangle = 4$  data. The data in the second column has been adapted from Figure 3 of ref 5. It should be noted that the data in column 2 includes an error bar of about  $\pm 0.03$ . <sup>b</sup> Data from ref 4 at 300K. <sup>c</sup> Data from ref 5 at an average energy of 0.5 eV. <sup>d</sup> Data from ref 8 at an average energy of 0.554 eV.

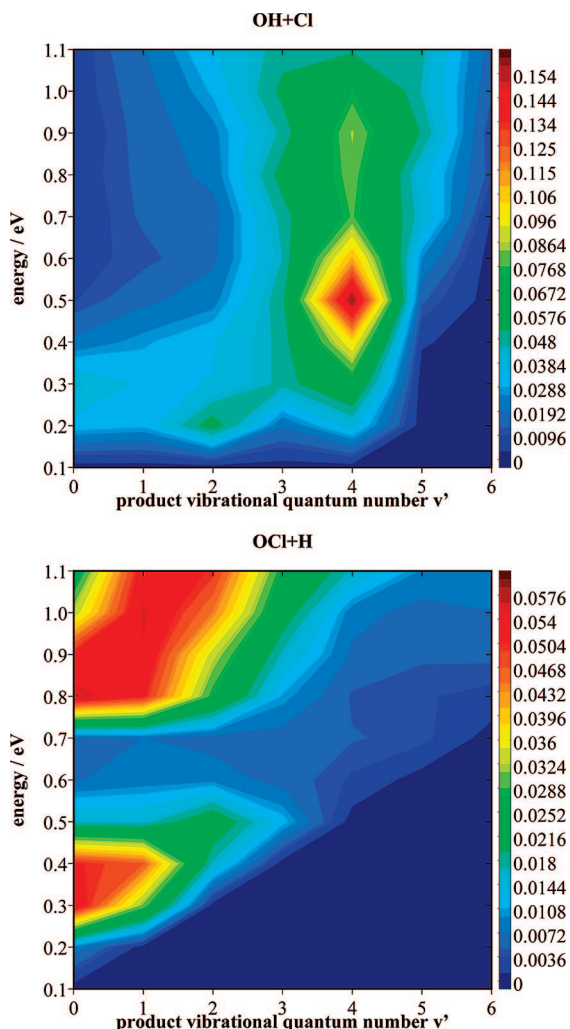
can be explained by the fact that the  $1\text{ }A''$  electronic state shows an early barrier for the production of  $\text{OH} + \text{Cl}$ .

Figure 3d shows the vibrational state resolved reaction probabilities for the  $\text{OCl} + \text{H}$  arrangement channel on the  $1\text{ }A''$  state PES. Probabilities for  $v' = 1-5$  are shown. The probabilities for all vibrational states shown are zero for energies below 0.65 eV.  $v' = 0$  is the most populated state for energies below 0.87 eV, and the probability decreases rapidly above this energy. Above 0.87 eV, the probability for  $v' = 1$  is the largest, and its magnitude is relatively constant for the whole energy range shown. The probabilities for  $v' = 2, 3, 4, 5$  rise continuously above the threshold for the whole energy range, with the ones for  $v' = 2$  and  $v' = 3$  becoming larger than the  $v' = 0$  probability above 0.96 and 1.06 eV respectively.

Figure 3e shows the reaction probabilities for the production of  $\text{OH} + \text{Cl}$  in vibrational states  $v' = 1-5$  for the  $2\text{ }A'$  state. Probabilities for vibrational states  $v' = 0-4$  are zero below 0.2 eV, whereas the one for  $v' = 5$  is zero below 0.34 eV (which is the same value as for the  $1\text{ }A'$  and  $1\text{ }A''$  electronic state). The reaction probabilities for  $v' = 1, 2, 3, 5$  rise linearly above the threshold for the whole energy range shown. The probability for  $v' = 4$  rises fast between 0.25 and 0.4 eV and starts to decrease above 0.53 eV. As for the  $1\text{ }A''$  electronic state PES, the  $2\text{ }A'$  electronic state PES has an early barrier for the production of  $\text{OH}$  giving rise to the vibrationally excited products.

Table 1 presents some of the available experimental data for the  $\text{OH}$  and  $\text{OCl}$  product vibrational state distributions. Presented in the table are those results that could be gleaned from figures or direct numbers from tables or text. Both experimental  $\text{OH}$  vibrational state distributions from Kruus et al.<sup>4</sup> and Park et al.<sup>5</sup> are inverted peaking at  $v' = 3, 4$ . The  $\text{OCl}$  vibrational distributions from Matsumi et al.<sup>8</sup> are not inverted peaking at  $v' = 0$ .

The results in panel (a) agree very well with the available experimental data for  $\text{OH}$  production. It is noteworthy that not only is the inversion with a peak at  $v' = 4$  reproduced (above an energy of 0.4 eV) but also that the peak is very pronounced with the probability of producing the other quantum states, besides  $v' = 3, 4, 5$ , being much smaller. For energies below 0.4 eV, the distributions show a less-pronounced peak with equal populations for  $v' = 2, 3, 4$  and the ones for  $v' = 0, 1$  only slightly smaller. The results for  $\text{OCl}$  are also in good agreement with the available experimental data showing a distribution with  $v' = 0$  being the most populated quantum state with the population decreasing with increasing  $v'$ . The  $\text{OCl}$  vibrational state distributions are fairly independent of energy. Only for



**Figure 4.** Vibrational product state distributions versus total energy in eV for both product arrangement channels averaged over all three electronic states. For the OH + Cl product channel contours are drawn between 0–0.16 in steps of 0.0032. For the OCI + H product channel contours are drawn between 0–0.06 in steps of 0.0012.

energies above 0.8 eV does this picture change with the population of  $v' = 5, 6$  being the highest leading to an inverted distribution.

The agreement of the OH vibrational distributions with experiment even for low energies improves when the excited electronic states are taken into account. The top panel of Figure 4 shows the average OH vibrational state distributions using equal weights for the three contributing electronic states. The contributions from the  $1\ A''$  and  $2\ A'$  electronic states increase the population of  $v' = 3$  and  $v' = 4$ , especially for energies below 0.4 eV giving rise to the pronounced peak at  $v' = 4$ . The peak broadens for higher energies with the populations for  $v' = 3$  and  $v' = 5$  steadily increasing while the population for  $v' = 4$  decreases. Experimental OH vibrational state distributions have been reported for 0.45<sup>11</sup> and 0.5 eV<sup>5</sup> (see also Table 1). The distributions at 0.5 eV shows a pronounced peak at  $v' = 4$  with the populations of  $v' = 3$  and  $v' = 2$  being about 2/3 of the one for  $v' = 4$  and the one for  $v' = 1$  being very small. The distribution at 0.45 eV peaks at  $v' = 3, 4$  with the population of  $v' = 0$  is negligible. The distributions calculated in the current work at these two energies show the highest population at  $v' = 4$  with the one for  $v' = 3$  and  $v' = 2$  being smaller. The populations for  $v' = 1$  and  $v' = 0$  are very small. The agreement for the two lowest vibrational states is due to the contributions

of the excited states and are therefore considered to be important and should be included in future theoretical studies of the OH product.

The OCI vibrational distributions change significantly if the contribution of the  $1\ A''$  state is taken into account, see bottom panel of Figure 4. The population of the lower vibrational states will be increased again leading to a statistical vibrational state distribution. Only for energies above 0.9 eV will the peak shift to  $v' = 1$ . Matsumi et al.<sup>8,9</sup> reported vibrational product state distributions at an energy of 0.554 eV (see also Table 1). The distribution shows that the population of  $v' = 0$  is nearly twice as large as that of  $v' = 1$  and that the one for  $v' = 2$  is about half of that of  $v' = 1$ . The population of  $v' = 3$  is zero. While the OCI distribution in Figure 4 shows agreement with this observation for energies below 0.5 eV and above 0.7 eV, the distribution taken around 0.55 eV shows a different picture. The highest population appears for  $v' = 2$  with  $v' = 0, 1, 3$  having very similar populations. The population for  $v' = 4$  is very close to zero. The contribution of the excited electronic states is zero at this energy, so these results are from the ground electronic state alone. While the N2 surfaces produce very good agreement with experiment for the OCI product vibrational state distributions for energies up to 0.5 eV and again above 0.7 eV for a narrow energy range, they give a relatively flat distribution showing a slight inversion peaking at  $v' = 2$ .

**C. Product Rotational Quantum State Distributions.** Figure 5 shows the product rotational state distributions obtained for the first six OH vibrational levels of the OH + Cl product channel on the ground electronic state  $1\ A'$  PES. The scale of the probability range is the same for all vibrational states. It is clear from the figure that the rotational state distributions are very localized for each vibrational quantum number. For  $v' = 0$ , rotational states between  $j' = 20$  and  $j' = 30$  are populated. This range does not change with increasing energy. The drop off above 0.4 eV is due to the significant decrease in magnitude of the reaction probability for the  $v' = 0$  product vibrational state (see Figure 3a). The same is true for  $v' = 1$  and  $v' = 2$ . For  $v' = 4$  and  $v' = 3$ , the magnitude is significant over the whole energy range, whereas for  $v' = 5$ , the magnitude of the rotational state populations is still increasing at 1.1 eV. The range of populated rotational states shifts to lower rotational quantum numbers with increasing vibrational quantum number. The results are in good agreement with the available experimental data.

Figure 6 shows the product rotational quantum state distributions for the OCI + H product channel obtained for the ground electronic state,  $1\ A'$ . It should be noted that the probability scale is smaller for  $v' = 3, 4, 5$ . The rotational state distributions are far less localized and are, in fact, spread out over nearly the whole energetically available range of rotational states. Low and high rotational states are equally populated. Here, the distributions do not shift to lower rotational states with higher vibrational quantum numbers. The populations of the rotational quantum states are zero for lower energies, but as soon as enough energy is available to populate a specific vibrational state, rotational levels for both low and high quantum numbers are populated. As for the OH rotational state distributions for this electronic state, the OCI rotational state distributions do not change significantly with increasing energy, and approximately the same range of states is populated for the entire energy range examined. We will see that this behavior is even more pronounced for the OCI rotational state distributions for the two excited electronic states.

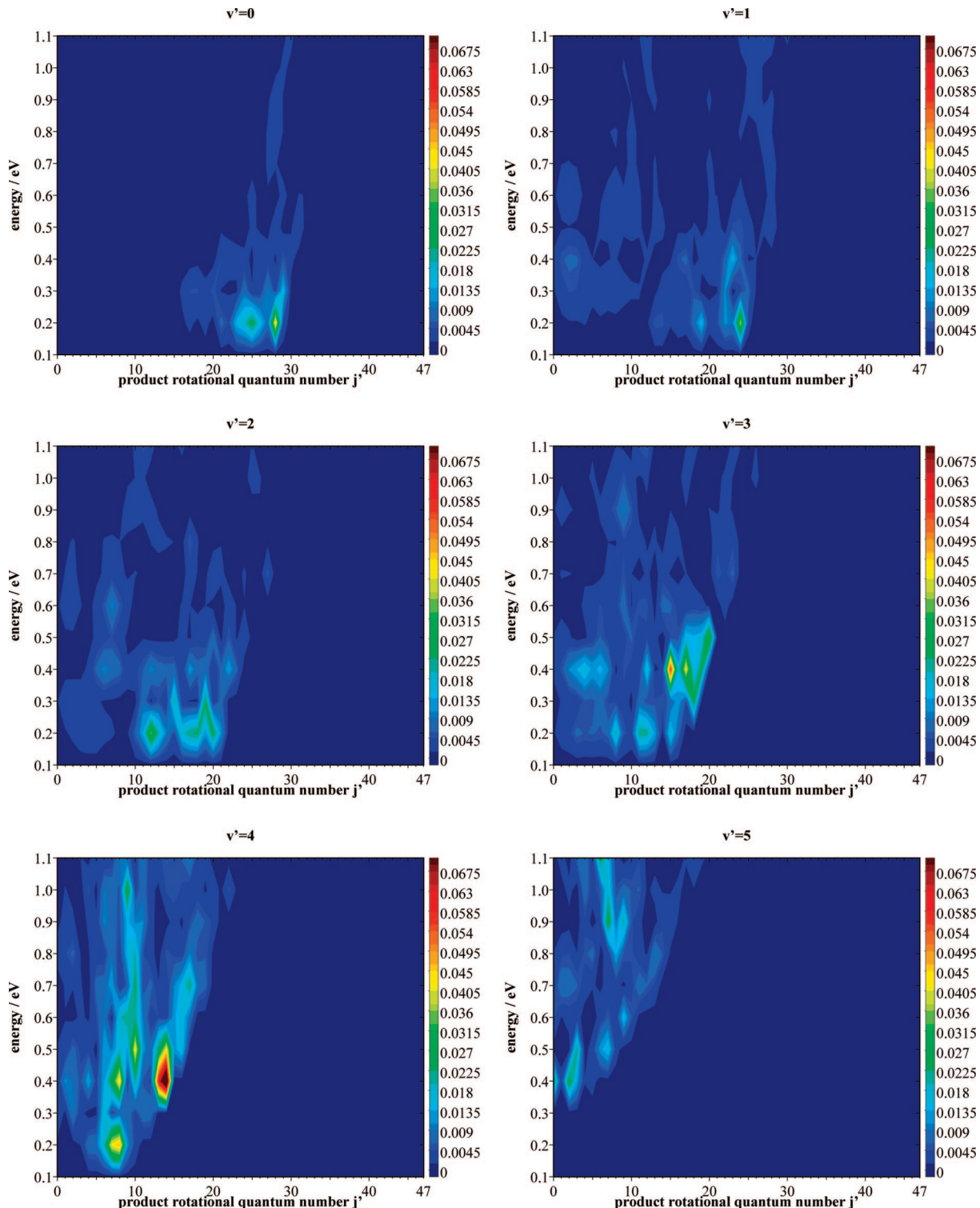


**Figure 5.** Rotational state distributions versus total energy in eV for the first six product vibrational states for the OH + Cl product channel on the  $1\text{ }A'$  electronic state. The scaling is the same for all panels, with contours between 0–0.07 in steps of 0.0015.

Figure 7 shows the rotational quantum state distributions for the OH + Cl product calculated using the  $1\text{ }A''$  electronic state PES. The probability scale is different (smaller) for  $v'=0$  and  $v'=1$ . For all vibrational states, only a very narrow range of rotational states are populated which is between  $j'=20$  to  $j'=30$  for  $v'=0$ ,  $j'=15$  to  $j'=25$  for  $v'=1$ ,  $j'=10$  to  $j'=20$  for  $v'=2$  and  $v'=3$  and  $j'=5$  to  $j'=15$  for  $v'=4$  and  $v'=5$ . The range of rotational energy levels populated shifts to smaller rotational quantum numbers with increasing product vibrational quantum number  $v'$ . The range of rotational states

populated gets slightly larger with increasing energy for all vibrational state. Specifically for  $v'=0$  and  $v'=1$ , and to some extend for  $v'=3$ , the range of populated rotational states spreads more to the lower rotational states for high energies.

Figure 8 shows the product rotational quantum state distributions for the OCl + H product on the  $1\text{ }A''$  electronic state PES. The rotational state distributions on this surface are very different from those produced by reaction on the  $1\text{ }A'$  electronic state PES. Note that the probability scale is different for  $v'=4$  and  $v'=5$ . Similar to results shown in some of the previous figures,

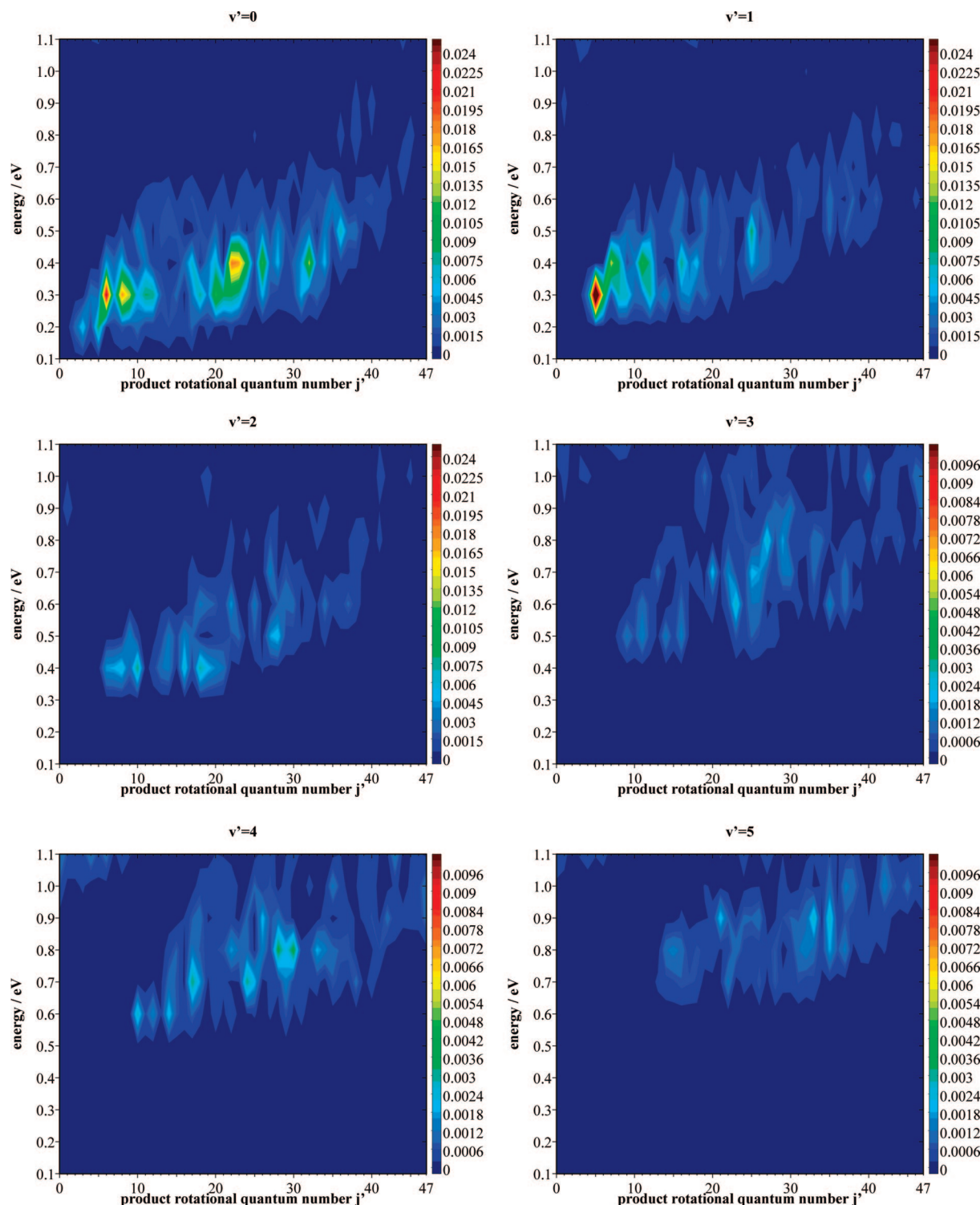


**Figure 6.** Rotational state distributions versus total energy in eV for the first six product vibrational states for the  $\text{OCl} + \text{H}$  product channel on the  $1 A'$  electronic state. For  $v' = 0-2$  contours are drawn between 0–0.025 in steps of 0.0005. The scaling is smaller for  $v' = 3-5$  with contours between 0–0.01 in steps of 0.0002.

the range of populated rotational states is narrow, but here only the lowest states are populated, mainly up to  $j' = 10$ . The range of rotational quantum numbers does not change significantly with increasing energy. The distributions also look much smoother than those previously examined and display just a single peak. For  $v' = 4$  and  $v' = 5$ , the overall reaction probability is considerably smaller than for the lower vibrational states, but we see that for very high energies, high rotational states are populated, but with low probability, and the distribu-

tions look less smooth than those for the other vibrational states and for lower energies. For  $v' = 0-2$ , the distributions slowly extend to higher rotational states with increasing energy but remain smooth, still showing a very pronounced peak for very low rotational states.

Figure 9 shows the OH product rotational quantum state distributions for reaction on the  $2 A'$  electronic state PES. The picture is similar to that produced by reaction on the  $1 A''$  electronic state PES. Note that the probability scale is different

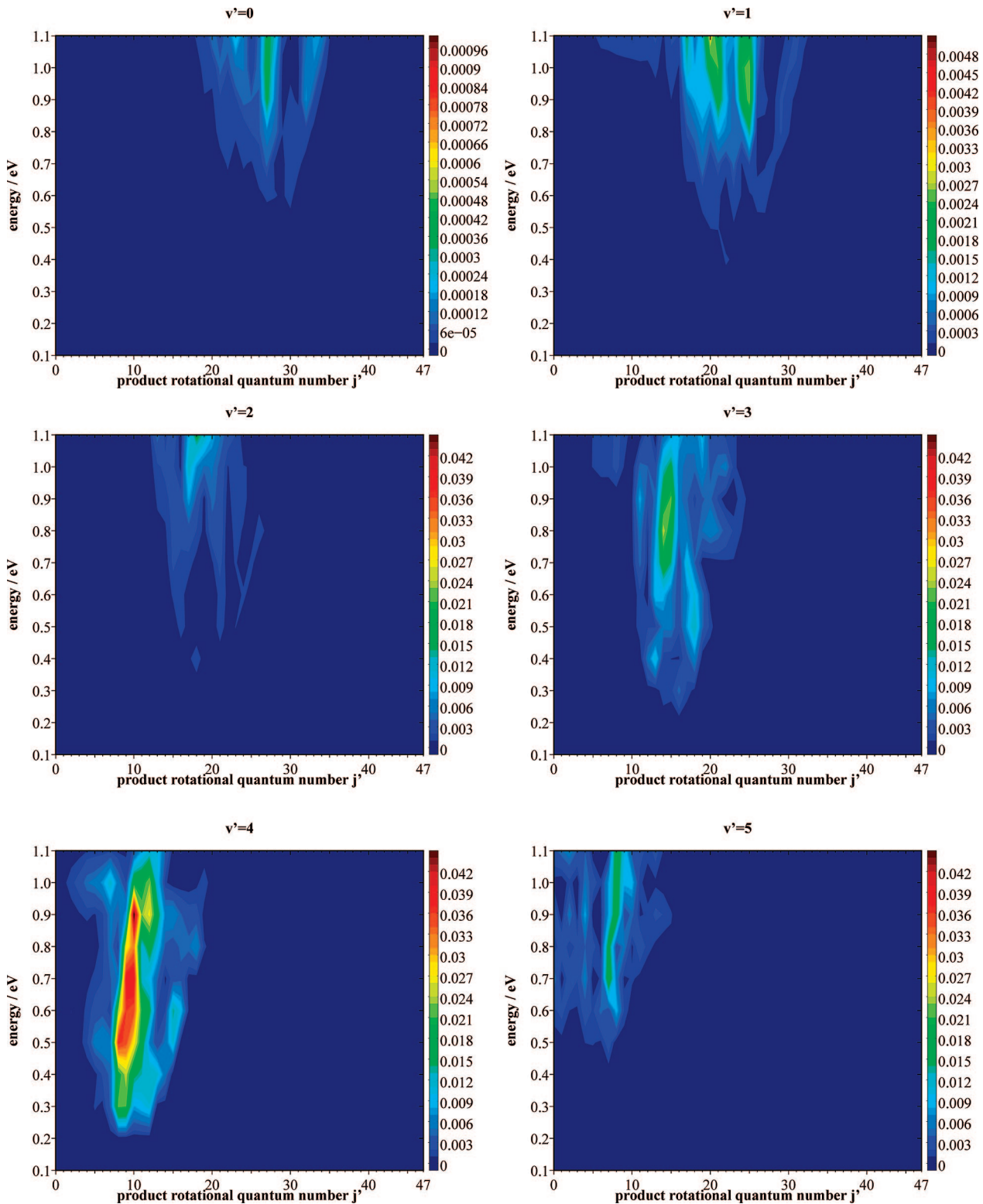


**Figure 7.** Rotational state distributions versus total energy in eV for the first six product vibrational states for the OH + Cl product channel on the 1  $A''$  electronic state. For  $v' = 2-5$  contours are drawn between 0–0.045 in steps of 0.001. The scale for  $v' = 1$  and  $v' = 0$  is smaller with contours between 0–0.005 in steps of 0.0001 for  $v' = 1$  and contours between 0–0.001 in steps of 0.00002 for  $v' = 0$ .

for  $v' = 0$  and  $v' = 5$ . The range of rotational states populated is similar for  $v' = 2-4$ , between  $j' = 10$  and  $j' = 20$ . The range for  $v' = 5$  is much narrower, located around  $j' = 10$ , whereas the range for  $v' = 0$  and  $v' = 1$  is between  $j' = 12$  and  $j' = 22$ . For all vibrational states, the range of rotational states populated slowly widens with increasing energy.

Figures 10 and 11 show the OH and OCl rotational distributions averaged over the three contributing electronic states. The

picture for the OH product rotational state distributions does not change if the contributions of all three electronic states are taken into account. As can be seen from Figure 10, the range of populated rotational states is similar to those found for the ground electronic state alone. Existing peaks and structures are enhanced, and the picture that mostly high rotational states are populated is reinforced. Figure 11 shows that for OCl inclusion of the excited electronic states changes the rotational state

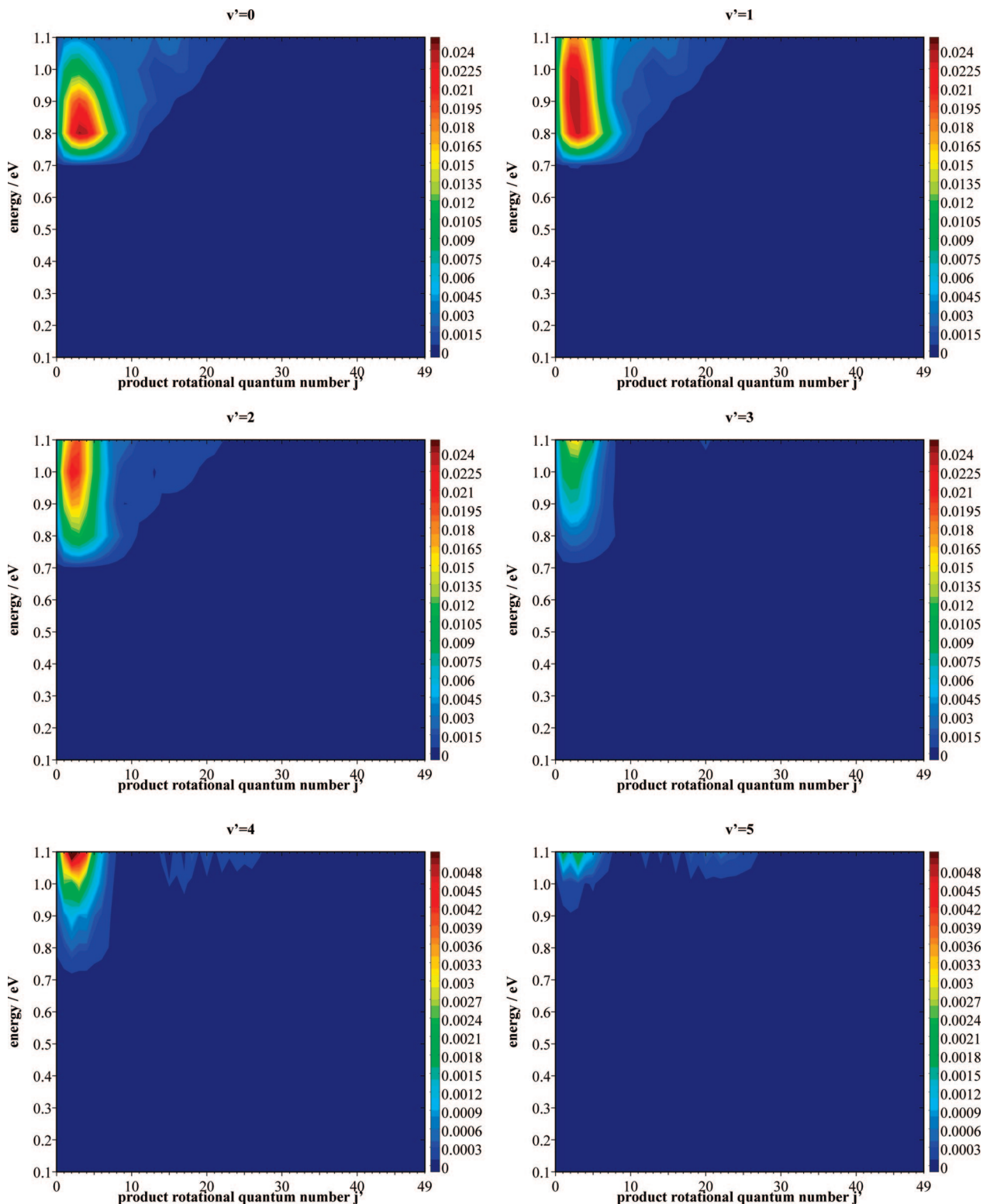


**Figure 8.** Rotational state distributions versus total energy in eV for the first six product vibrational states for the OCl + H product channel on the 1  $A''$  electronic state. For  $v' = 0\text{--}3$  contours are drawn between 0–0.025 in steps of 0.0005. The scale for  $v' = 4$  and  $v' = 5$  is smaller with contours drawn between 0–0.005 in steps of 0.0001.

distributions for the higher energies. For energies below 0.7 eV, the results compare well with the experimental data and show that all accessible rotational states are evenly populated. For energies above 0.7 eV however, the distributions shift to mainly very low rotational states showing a single very pronounced peak. To date, no experimental study has reported rotational state distributions at such high energies.

#### IV. Conclusions

We have presented quantum reactive scattering calculations for the O( $^1D$ ) + HCl system employing the N<sub>2</sub> PESs and the real wavepacket approach. Branching ratios have been calculated as a function of energy, taking account of reaction simultaneously on three electronic state potential energy surfaces. For

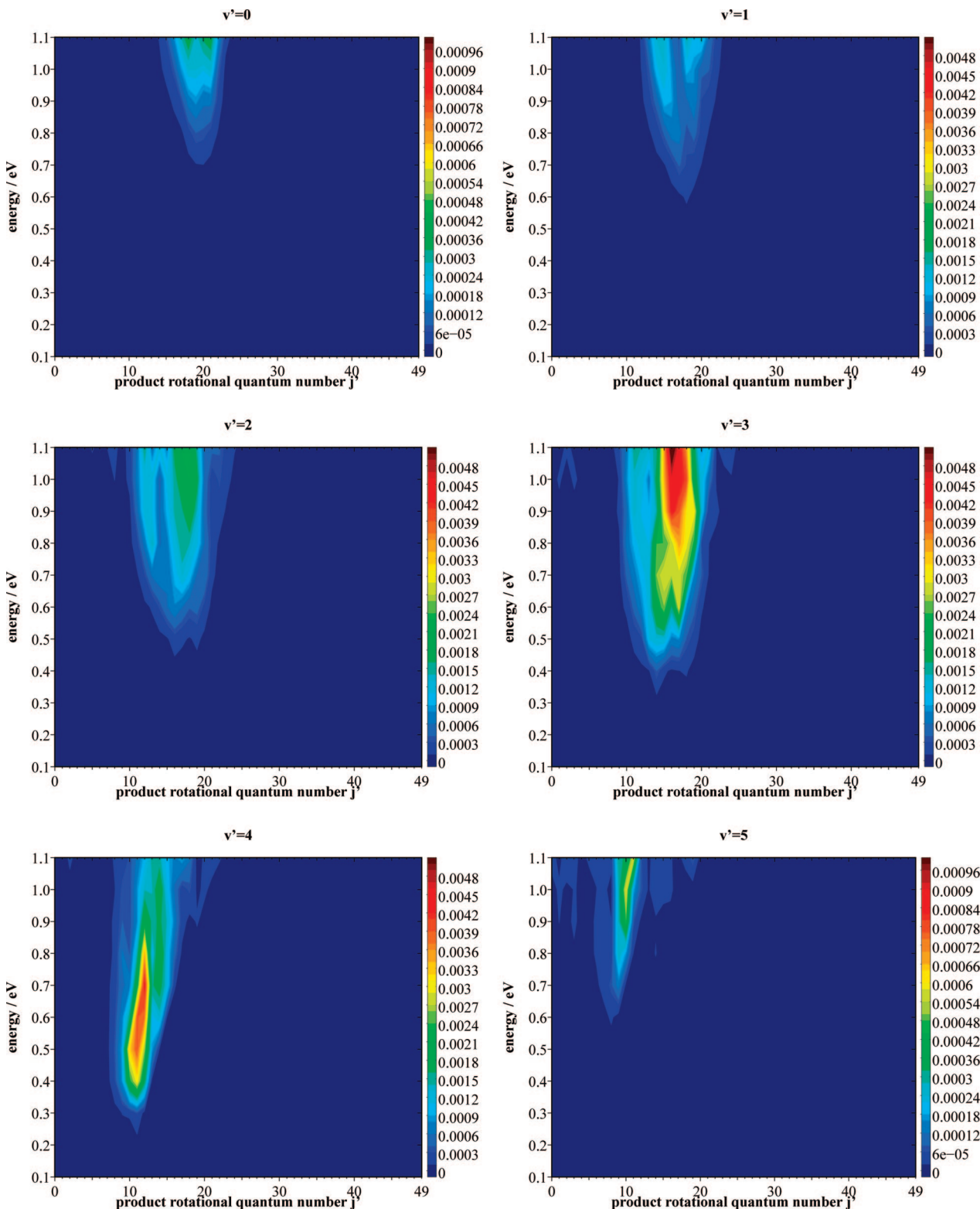


**Figure 9.** Rotational state distributions versus total energy in eV for the first six product vibrational states for the OH + Cl product channel on the  $2 A'$  electronic state. For  $v' = 1-4$  contours are drawn between 0–0.005 in steps of 0.0001. The scale for  $v' = 0$  and  $v' = 5$  is smaller with contours between 0–0.001 in steps of 0.00002.

comparison purposes, the branching ratio obtained using only the lowest electronic state PES has also been presented. The branching ratio obtained from the ground electronic state only is in excellent agreement with the available experimental results. Including the contributions from the excited electronic states significantly changes the branching ratios for energies above 0.7 eV. However, the branching ratio below this threshold is

still in good agreement with the experimental values. At energies above 0.7 eV, the computed branching ratio increases significantly (see Figure 2) due to the contribution of the  $1 A''$  state to the OCl + H reaction probability. It would be interesting to see if experiments at higher energies would show the same significant rise of the branching ratio above 0.7 eV as the current theoretical predictions.

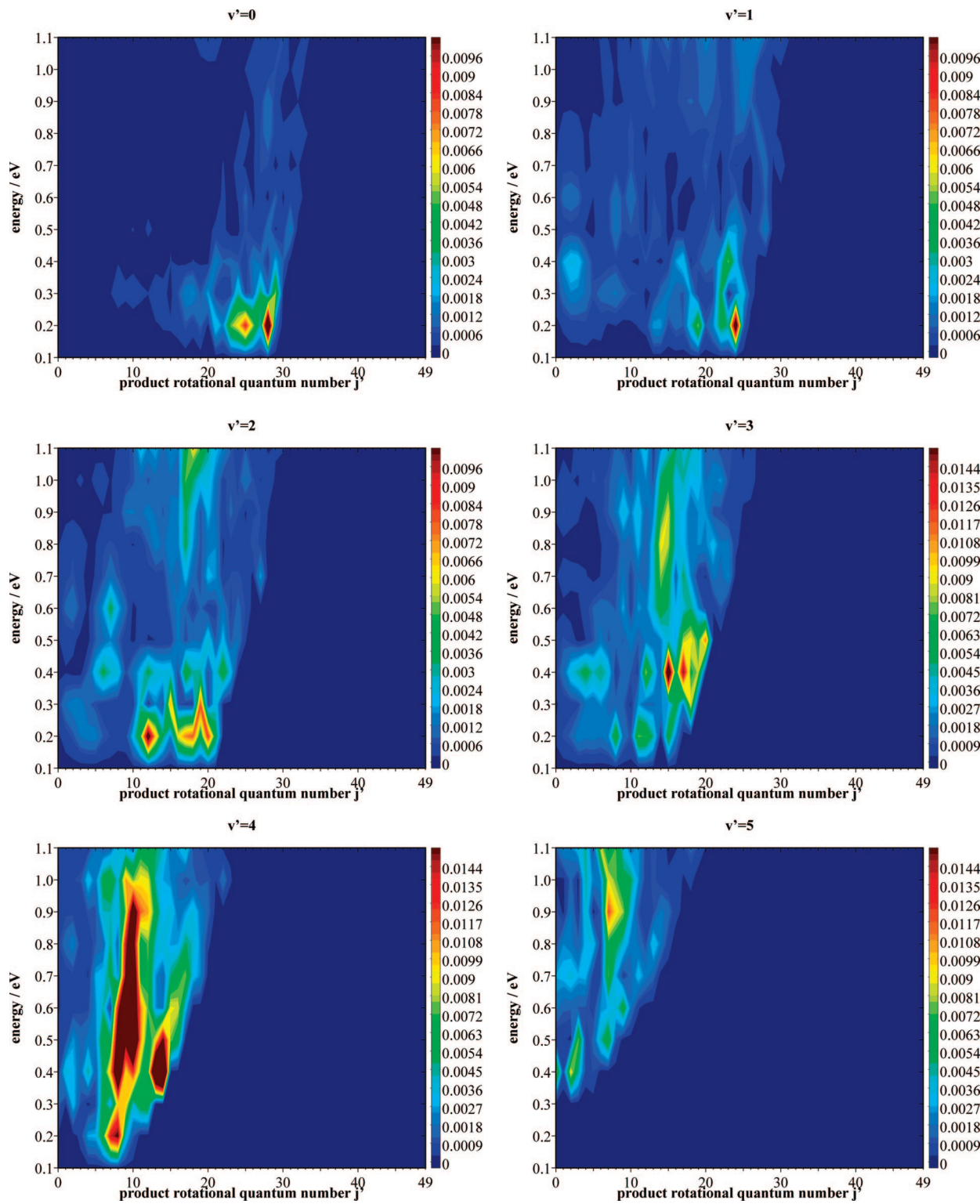


**Figure 10.** Rotational state distributions versus total energy in eV for the first six product vibrational states for the OH + Cl product channel averaged over all three electronic states. For  $v' = 0\text{--}2$  contours are drawn between 0–0.001 in steps of 0.00002. The scale for  $v' = 3\text{--}5$  is larger with contours between 0–0.0015 in steps of 0.00005.

We have also presented reaction probabilities for the formation of the different product vibrational states as a function of energy. The OH vibrational state distributions ( $1\text{A}'$  only and taking account of all three electronic states) shows a pronounced peak at  $v' = 4$ , in excellent agreement with all of the available experimental results. Including the contributions of the excited electronic states causes the peak to become broader with increasing energy. The OCl product vibrational quantum state

distributions peak at  $v' = 0$  with the population decreasing with increasing  $v'$ . Contributions from the excited electronic state reinforce this picture, and only for very high energies does the peak shift to  $v' = 1$ . At these high energies and in the range between 0.5 to 0.7 eV, the populations of all states are similar, leading to a broad and relatively flat distribution. These results are in reasonably good agreement with the available experimental data.

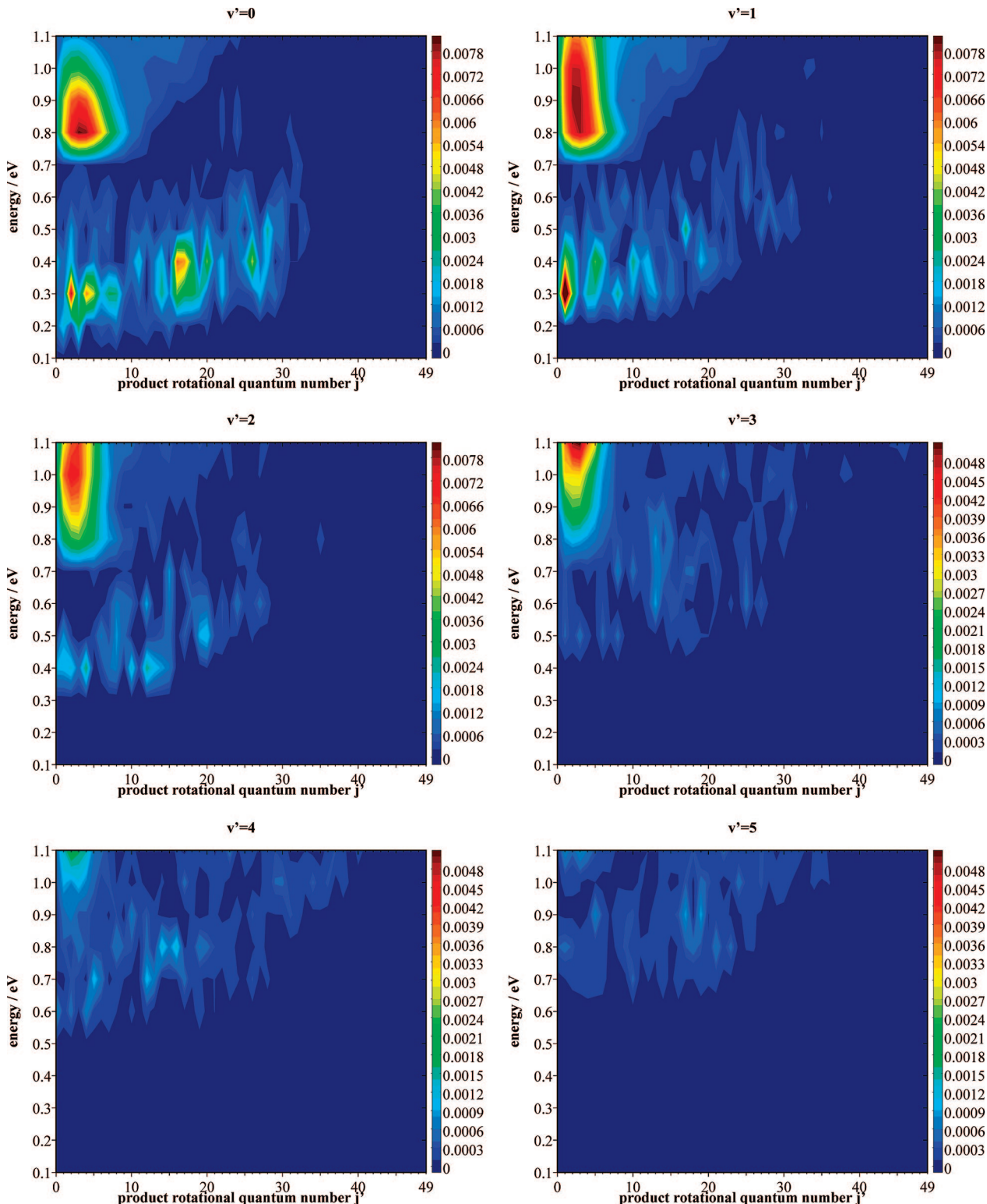


**Figure 11.** Rotational state distributions versus total energy in eV for the first six product vibrational states for the OCl + H product channel averaged over all three electronic states. For  $v' = 0-2$  contours are drawn between 0–0.008 in steps of 0.00016. The scale for  $v' = 3-5$  is smaller with contours between 0–0.005 in steps of 0.00001.

The OH product rotational quantum state distributions are highly localized to a small range of high rotational states. The range shifts to lower rotational quantum numbers with increasing  $v'$  but is mainly independent of energy. Including the contributions from the excited electronic states reinforces this picture. The available experimental data, mainly for  $v' = 2, 3, 4$ , agree well with our findings. The OCl rotational state distributions on the  $1\ A'$  electronic state only are very broad with all rotational

states equally populated. Again, the range of rotational states populated is independent of energy. In this case, the contributions from the excited electronic state will significantly change the distributions for high energies mainly populating the very low  $j'$  rotational quantum states.

The current study raised several questions as to the contribution of the  $1\ A''$  excited electronic state especially to the dynamics of the OCl + H channel. These contributions not only

significantly change the branching ratio, but also the rotational distributions above 0.7 eV.

All results presented here are for total angular momentum  $J = 0$  and for the ground-state of the reactants ( $v = 0, j = 0$ ) only. While our current study shows very good agreement with the experimental data, a more realistic comparison with experiment should include the average over all accessible initial states, over all partial waves ( $J$  values), and should also include nonadiabatic coupling between the different electronic states. Theoretical studies have found a small effect of initial rotational excitation on the branching ratio leading to an increase.<sup>29,31,32</sup> To our knowledge, no theoretical study investigating the effect of initial state excitation on the product state distribution has been reported to date. Quantum mechanical calculations for  $J > 0$  have been carried out employing the centrifugal sudden approximation<sup>27,28</sup> but no full Coriolis coupled calculations have been reported so far. Such calculations will be extremely difficult. As can be seen from Table 1 in our paper I,<sup>41</sup> several wavepackets are necessary to cover a reasonable energy range and very dense grids are needed. We hope to perform calculations in the future that will establish whether it is necessary to include  $J > 0$  and excited initial ro-vibrational states to obtain reliable predictions for this system.

**Acknowledgment.** The calculations reported in this work have been performed on the CMS computational facility housed by the Centre for Computational Molecular Science, Australian Institute for Bioengineering and Nanotechnology, University of Queensland, Australia. These computational facilities have been purchased from funds provided by the University of Queensland and the Queensland Smart State Research Facilities Fund. M.H. would like to thank Sun Microsystems and the University of Queensland for funding. H.Y. acknowledges financial support from The University of Queensland during a research visit to the Centre for Computational Molecular Science, April–July 2007. The real wavepacket computer codes used in the work were developed in collaboration with S. K. Gray.

## References and Notes

- (1) Basco, N.; Norrish, R. G. W. *Proc. R. Soc. London, Ser. A* **1961**, 260.
- (2) Luntz, A. C. *J. Chem. Phys.* **1980**, 73, 1143.
- (3) Wine, P. H.; Wells, J. R.; Ravishankara, A. R. *J. Chem. Phys.* **1986**, 84, 1349.
- (4) Kruus, E. J.; Niefer, B. I.; Sloan, J. J. *J. Chem. Phys.* **1988**, 88, 985.
- (5) Park, C. R.; Wiesenfeld, J. R. *Chem. Phys. Lett.* **1989**, 163, 230.
- (6) Balucani, N.; Beneventi, L.; Casavecchia, P.; Volpi, G. G. *Chem. Phys. Lett.* **1991**, 180, 34.
- (7) Matsumi, Y.; Tonokura, K.; Kawasaki, M.; Tsuji, K.; Obi, K. *J. Chem. Phys.* **1993**, 98, 8330.
- (8) Matsumi, Y.; Shamsuddin, S. M.; Kawasaki, M. *J. Chem. Phys.* **1994**, 101, 8262.
- (9) Matsumi, Y.; Shamsuddin, S. M. *J. Chem. Phys.* **1995**, 103, 4490.
- (10) Alexander, A. J.; Brouard, M.; Rayner, S. P.; Simons, J. P. *Chem. Phys.* **1996**, 207, 215.
- (11) Kohguchi, H.; Suzuki, T. *Chem. Phys. Chem.* **2006**, 7, 1250.
- (12) Kohguchi, H.; Suzuki, T.; Nanbu, S.; Ishida, T.; Mil'nikov, G. V.; Oloyede, P.; Nakamura, H. *J. Phys. Chem. A* **2008**, 112, 818.
- (13) Schinke, R. *J. Chem. Phys.* **1984**, 80, 5510.
- (14) Laganá, A.; Ochoa de Aspuru, G.; Gracia, E. *J. Phys. Chem.* **1995**, 99, 17139.
- (15) Hernández, M. L.; Redondo, C.; Laganá, A.; Ochoa de Aspuru, G.; Rosi, M.; Sgamellotti, A. *J. Chem. Phys.* **1996**, 105, 2710.
- (16) Skokov, S.; Peterson, K. A.; Bowman, J. M. *J. Chem. Phys.* **1998**, 109, 2662.
- (17) Alvariño, J. M.; Bolloni, A.; Hernández, M. L.; Laganá, A. *J. Phys. Chem. A* **1998**, 102, 10199.
- (18) Skokov, S.; Qi, J.; Bowman, J. M.; Yang, C.-Y.; Gray, S. K.; Peterson, K. A.; Mandelshtam, V. A. *J. Chem. Phys.* **1998**, 109, 10273.
- (19) Alvariño, J. M.; Rodríguez, A.; Laganá, A.; Hernández, M. L. *Chem. Phys. Lett.* **1999**, 313, 199.
- (20) Peterson, K. A.; Skokov, S.; Bowman, J. M. *J. Chem. Phys.* **1999**, 111, 7446.
- (21) Christoffel, K. M.; Kim, Y.; Skokov, S.; Bowman, J. M.; Gray, S. K. *Chem. Phys. Lett.* **1999**, 315, 275.
- (22) Martínez, T.; Hernández, M. L.; Alvariño, J. M.; Laganá, A.; Aoiz, F. J.; Menéndez, M.; Verdasco, E. *Phys. Chem. Chem. Phys.* **2000**, 2, 589.
- (23) Lin, S. Y.; Han, K.-L.; Zhang, J. Z. H. *Phys. Chem. Chem. Phys.* **2000**, 2, 2529.
- (24) Lin, S. Y.; Han, K.-L.; Zhang, J. Z. H. *Chem. Phys. Lett.* **2000**, 324, 122.
- (25) Bittererová, M.; Bowman, J. M. *J. Chem. Phys.* **2000**, 113, 1.
- (26) Bittererová, M.; Bowman, J. M.; Peterson, K. J. *Chem. Phys.* **2000**, 113, 6186.
- (27) Piermarini, V.; Balint-Kurti, G. G.; Gray, S. K.; Göktas, F.; Laganá, A.; Hernández, M. L. *J. Phys. Chem. A* **2001**, 105, 5743.
- (28) Piermarini, V.; Laganá, A.; Balint-Kurti, G. G. *Phys. Chem. Chem. Phys.* **2001**, 3, 4515.
- (29) Christoffel, K. M.; Bowman, J. M. *J. Chem. Phys.* **2002**, 116, 4842.
- (30) Nanbu, S.; Aoyagi, M.; Kamisaka, H.; Nakamura, H.; Bian, W.; Tanaka, K. *J. Theor. Comput. Chem.* **2002**, 1, 263.
- (31) Kamisaka, H.; Nakamura, H.; Nanbu, S.; Aoyagi, M.; Bian, W.; Tanaka, K. *J. Theor. Comput. Chem.* **2002**, 1, 275.
- (32) Kamisaka, H.; Nakamura, H.; Nanbu, S.; Aoyagi, M.; Bian, W.; Tanaka, K. *J. Theor. Comput. Chem.* **2002**, 1, 285.
- (33) Lin, S. Y.; Park, S. C. *Bull. Korean Chem. Soc.* **2002**, 23, 229.
- (34) Göktas, F.; Bulut, N.; Akpinar, S. *J. Mol. Struct.* **2003**, 625, 177.
- (35) Martínez, T.; Hernández, M. L.; Alvariño, J. M.; Aoiz, F. J.; SáezRábanos, V. *J. Chem. Phys.* **2003**, 119, 7871.
- (36) Bian, W.; Poirier, B. *J. Chem. Phys.* **2004**, 121, 4467.
- (37) All energies will be presented as total energies and are measured from the lowest point of the potential energy curve of the reactants.
- (38) Liu, B., unpublished data.
- (39) Zhang, H.; Smith, S. C.; Nanbu, S.; Nakamura, H. *J. Phys. Chem. A* **2006**, 110, 5468.
- (40) Zhang, H.; Hankel, M.; Smith, S. C.; Nanbu, S.; Nakamura, H. *J. Phys. Chem. A* **2008**, 112, 4141.
- (41) Yang, H.; Han, K.-L.; Nanbu, S.; Nakamura, H.; Balint-Kurti, G. G.; Zhang, H.; Smith, S. C.; Hankel, M. *J. Chem. Phys.* **2008**, 128, 014308.
- (42) Gray, S. K.; Balint-Kurti, G. G. *J. Chem. Phys.* **1998**, 108, 950.
- (43) Hankel, M.; Balint-Kurti, G. G.; Gray, S. K. *J. Chem. Phys.* **2000**, 113, 9658.
- (44) Hankel, M.; Balint-Kurti, G. G.; Gray, S. K. *J. Phys. Chem.* **2001**, 105, 2330.

JP803673Y